Supplementary information

Intercalation type pseudocapacitive clustered nanoparticles of nickel-cobalt phosphate thin films synthesized via electrodeposition as a cathode for high performing hybrid supercapacitor devices

Supriya J. Marje,[a] Sachin S. Pujari,[a] Suraj A. Khalate,[a] Vinod V. Patil,[a] Vinayak G. Parale,[b] Taehee kim,[b] Hyung-Ho Park,[b] Jayavant L. Gunjakar,[a] Chandrakant D. Lokhande,[a] Umakant M. Patil[a*]

[a]Centre for Interdisciplinary Research, D. Y. Patil Education Society (Deemed to be University), Kasaba Bawada, Kolhapur-416 006, M.S., India.
[b]Department of Materials Science and Engineering, Yonsei University, Seoul 03722, South Korea.

1. Synthesis of large area nickel-cobalt phosphate thin film

For potentiostatic electrodeposition, the conventional three-electrode system is used as an electrochemical cell consisting of flexible stainless steel (SS) as a working electrode, graphite pot as a counter electrode, and saturated calomel electrode (SCE) (saturated KCl solution) as a reference electrode. The schematic presentation and the actual setup of the large area thin film deposition assembly are presented in Fig. S1 (a) and (b), respectively. The photograph of the deposited large area of nickel-cobalt phosphate thin film is shown in Fig. S1 (c).

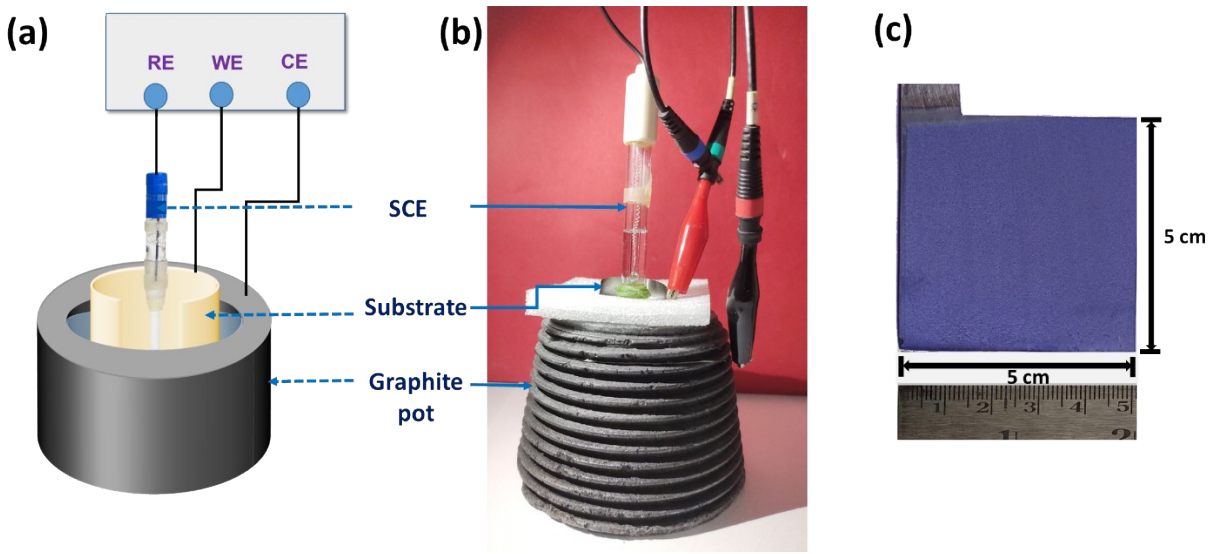

Fig. S1 (a) The schematic presentation, (b) photograph of large-area thin film deposition assembly, and (c) photograph of deposited large area (5x5 cm^2) nickel-cobalt phosphate thin film.

2. Synthesis of reduced graphene oxide (rGO)

The modified Hummer's method was employed for the preparation of graphene oxide,[S1] then reduced hydrothermally. The rGO electrode was prepared by adding active material (rGO) (75%), carbon black (20%), and polyvinylidene fluoride (5%) in N-methyl 2-pyrrolidone (NMP) solvent. The prepared slurry was coated on stainless steel substrate (1x1 cm^2), heated at 333 K for an hour, and used for further study.

3. Synthesis of PVA-KOH gel electrolyte

The PVA-KOH gel electrolyte was prepared for the fabrication of a solid-state device. The 3 g of polyvinyl alcohol (PVA) was dissolved in 30 ml of double-distilled water (DDW) at 363 K under vigorous stirring. The solution is continuously stirred up to complete dissolution of polymer in water and clear appearance of the solution. After that 10 ml of 1 M KOH solution was added to the PVA solution with continuous stirring and obtained a homogeneous, dense, and clear solution.[S2] The prepared transparent and viscous PVA-KOH was used as a gel electrolyte for the solid-state device fabrication.

4. Fabrication of solid-state hybrid asymmetric supercapacitor (SHAS) device

The SHAS device was fabricated by comprising E-NCP4 thin film as cathode and rGO electrode as anode with PVA-KOH as gel electrolyte and separator. The SHAS device fabrication steps are illustrated in Fig. S2 (a-d). In the first step, the large area flexible electrodes are prepared as shown in Fig. S2 (a) and used as electrodes to fabricate the SHAS device. Then, the gel electrolyte was painted on each electrode material and dried at room temperature (shown in Fig. S2 (b)). After drying, the edges of electrodes are sealed with plastic tape, as illustrated in Fig. S2 (c), to avoid a short circuit. Again, the gel electrolyte was painted on the surface of active material for proper contact between electrode and electrolyte. Then, the electrodes were packed together using transparent plastic strips. Later, the prepared device is pressed under hydraulic pressure of 0.5 tons for 12h. Photographs of prepared flexible SHAS device are shown in Fig. S2 (d) and the schematic presentation in Fig. S2 (e). The electrochemical performance of SHAS device was tested using ZIVE MP1 electrochemical workstation.

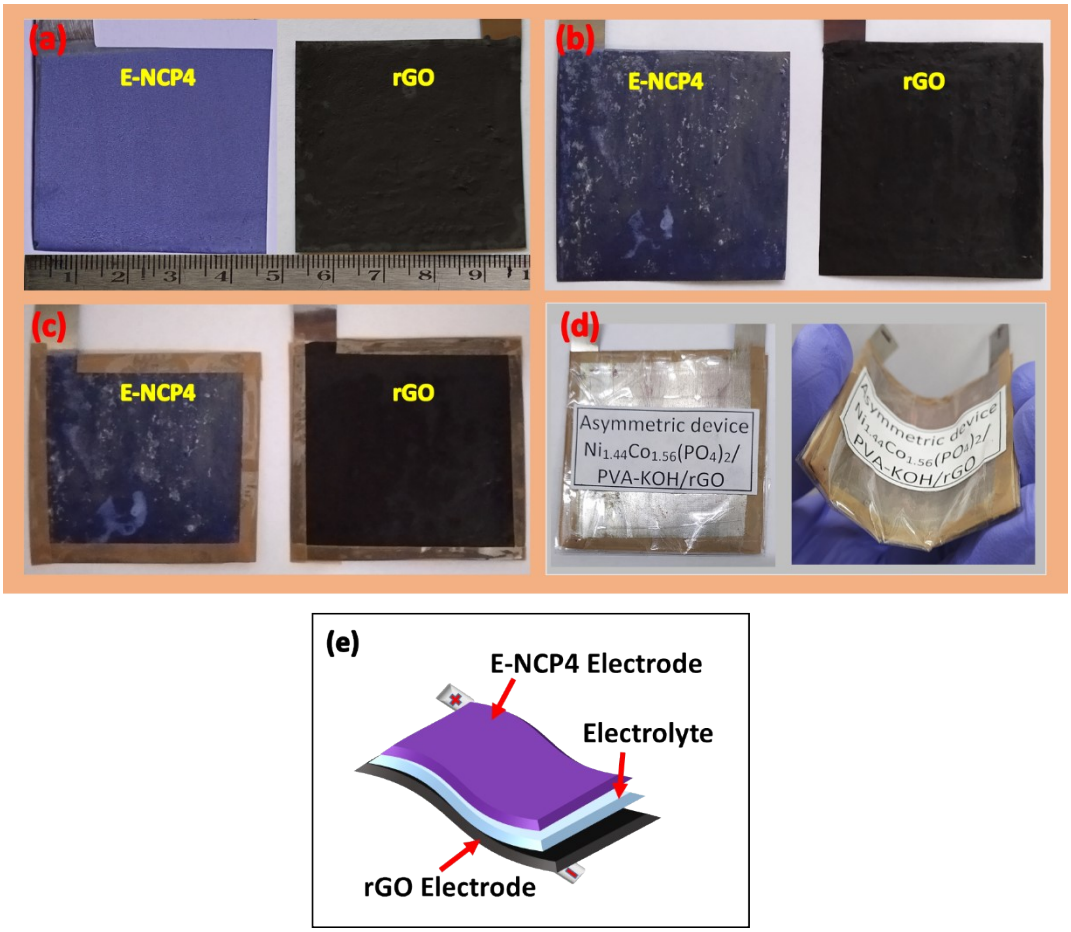

Fig. S2 The digital photographs of (a) E-NCP4 (electrodeposited) and rGO thin film electrodes on flexible stainless steel substrate, (b) electrodes painted by PVA-KOH gel electrolyte, (c) sealed edges with tape, and (d) fabricated flexible solid-state device. (e) Schematic presentation of flexible solid-state device.

5. Formulae for calculations

5.1 For three electrode system:

Specific capacitance is derived from GCD analysis as follows,

$$C_s = \frac{I \times \Delta t}{w \times \Delta V} \qquad (\text{F g}^{-1}) \qquad (S1)$$

where I, Δt, w and ΔV are current density, discharging time, mass of active material, and potential window, respectively. Furthermore, the specific capacity of electrode from the GCD analysis is measured as follows,

$$Q = \frac{I \times \Delta t}{w} \qquad (\text{C g}^{-1}) \qquad (S2)$$

Capacitive and diffusion-controlled processes are contributed to total charge storage of electrode, and according to Power's law, CV current is dependent on scan rate and can be expressed as follows,

$$i_p(v) = av_b \qquad (S3)$$

where, i_p, v, a and b are represent the peak current, scan rate, and adjustable parameters.

The modified Power's law is used for the calculation of respective current contribution from the diffusion-controlled process (bulk battery) and pseudocapacitive process as given below,

$$I_p = I_{surface} + I_{bulk} = C_{surface}v + C_{bulk}v^{1/2} \qquad (S4)$$

where I_p, v, $C_{surface}v$, and $C_{bulk}v^{1/2}$ represent the peak current density, scan rate, surface pseudocapacitive process ($I_{surface}$) current contribution, and bulk process (I_{bulk}) current contribution, respectively.

5.2 For two electrode system:

The charges between the cathode and anode can be balanced for excellent electrochemical results of hybrid asymmetric supercapacitor device by using the theory of mass balance as per the following equation,

$$\frac{m_+}{m_-} = \frac{C_- \times \Delta V_-}{C_+ \times \Delta V_+} \quad \text{(S5)}$$

where, $m_{(+\ or\ -)}$, $\Delta V_{(+ or -)}$, and $C_{(+ or -)}$ are the mass of active material (g), potential window (V), and specific capacitance (F g^{-1}) of positive and negative electrode, respectively.

The two electrode system was used to study device performance, and its energy (E) and power density (P) are calculated using following equations, respectively,

$$E = \frac{0.5 \times C_s \times (\Delta V)^2}{3.6} \quad \text{(Wh } kg^{-1}\text{)} \quad \text{(S6)}$$

And

$$P = \frac{E \times 3.6}{\Delta t} \quad \text{(kW } kg^{-1}\text{)} \quad \text{(S7)}$$

where C_s, ΔV, and Δt represent specific capacitance, potential window, and discharging time of device, respectively.

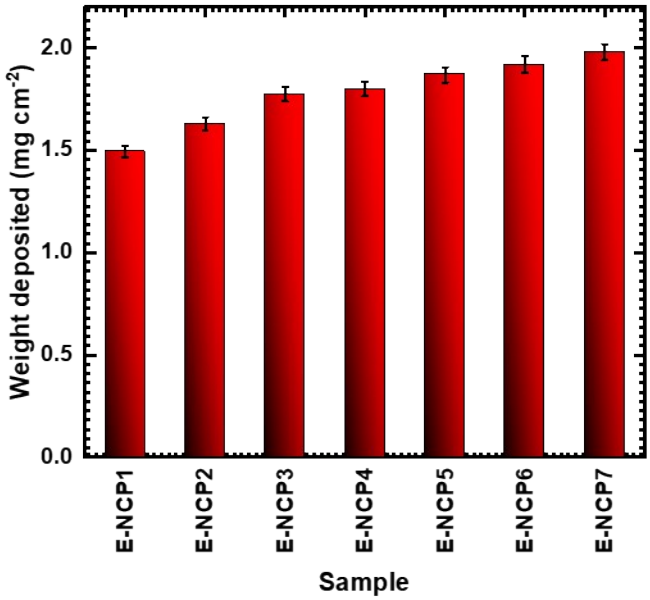

Fig. S3 Graph of nickel-cobalt phosphate thin film thickness at different compositions of Ni:Co.

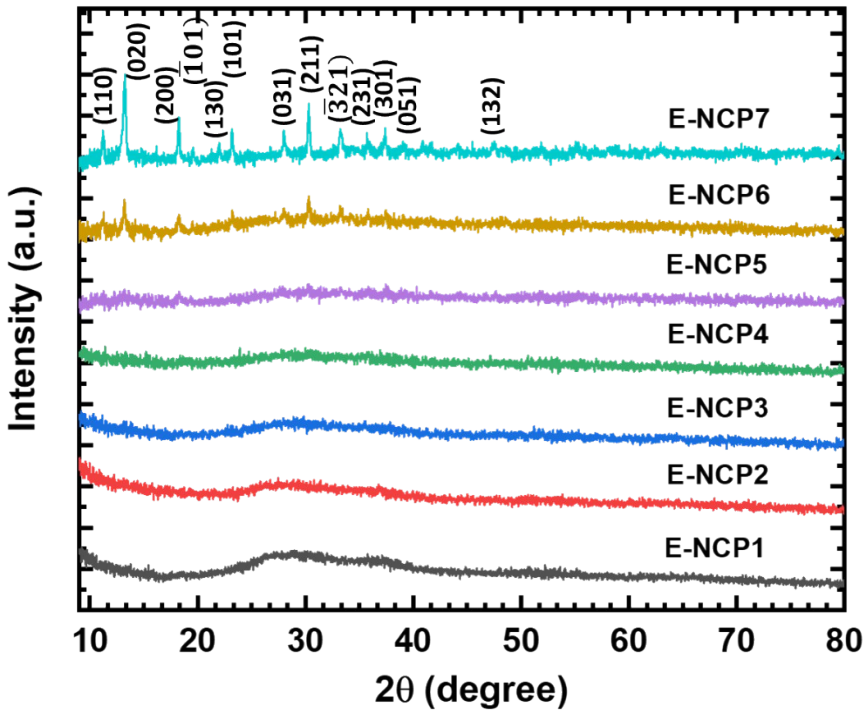

Fig. S4 XRD patterns of nickel-cobalt phosphate powder samples (E-NCP1 to E-NCP7).

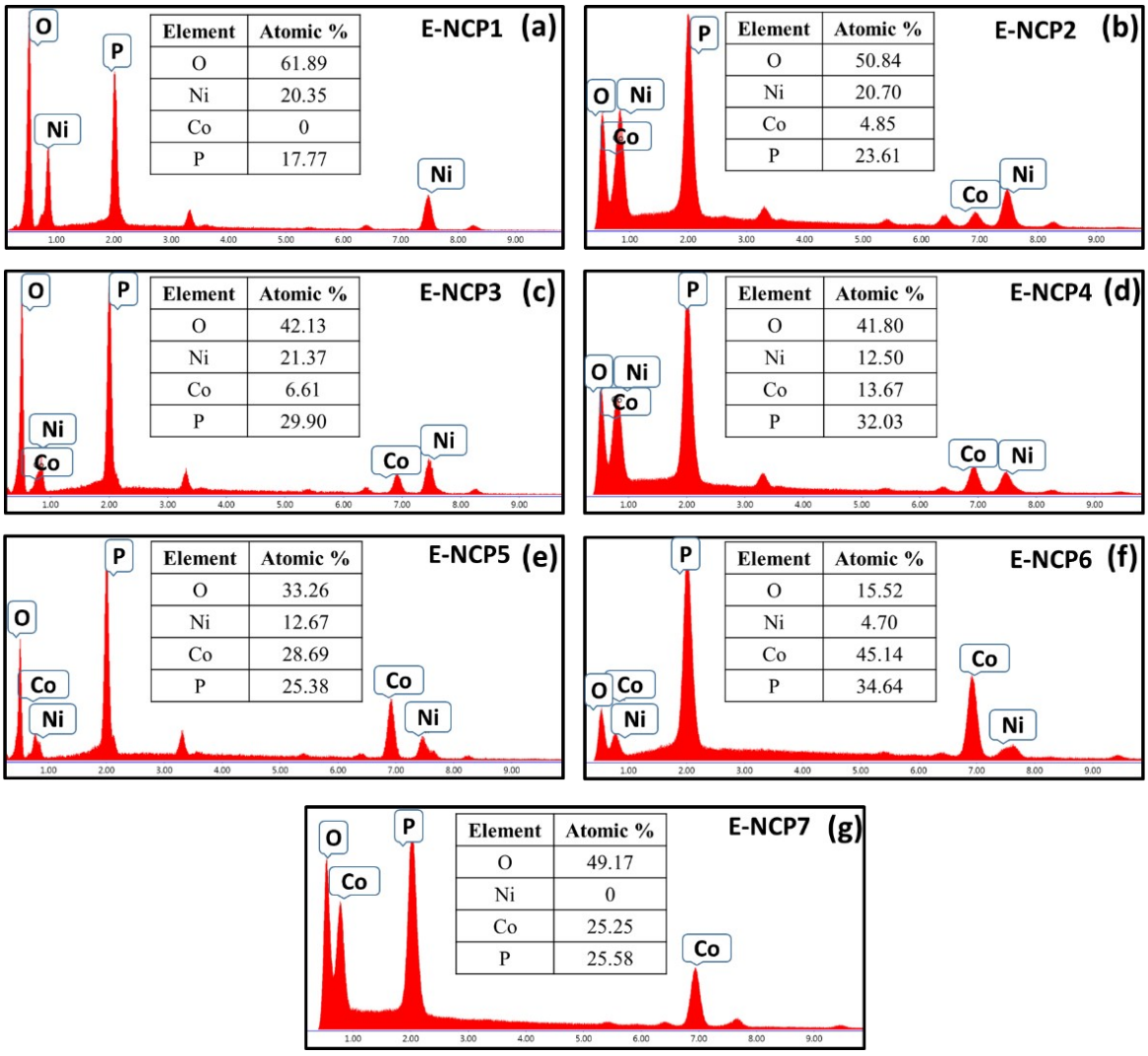

Fig. S5 EDS spectra of nickel-cobalt phosphate thin film samples (a) E-NCP1, (b) E-NCP2, (c) E-NCP3, (d) E-NCP4, (e) E-NCP5, (f) E-NCP6 and (g) E-NCP7.

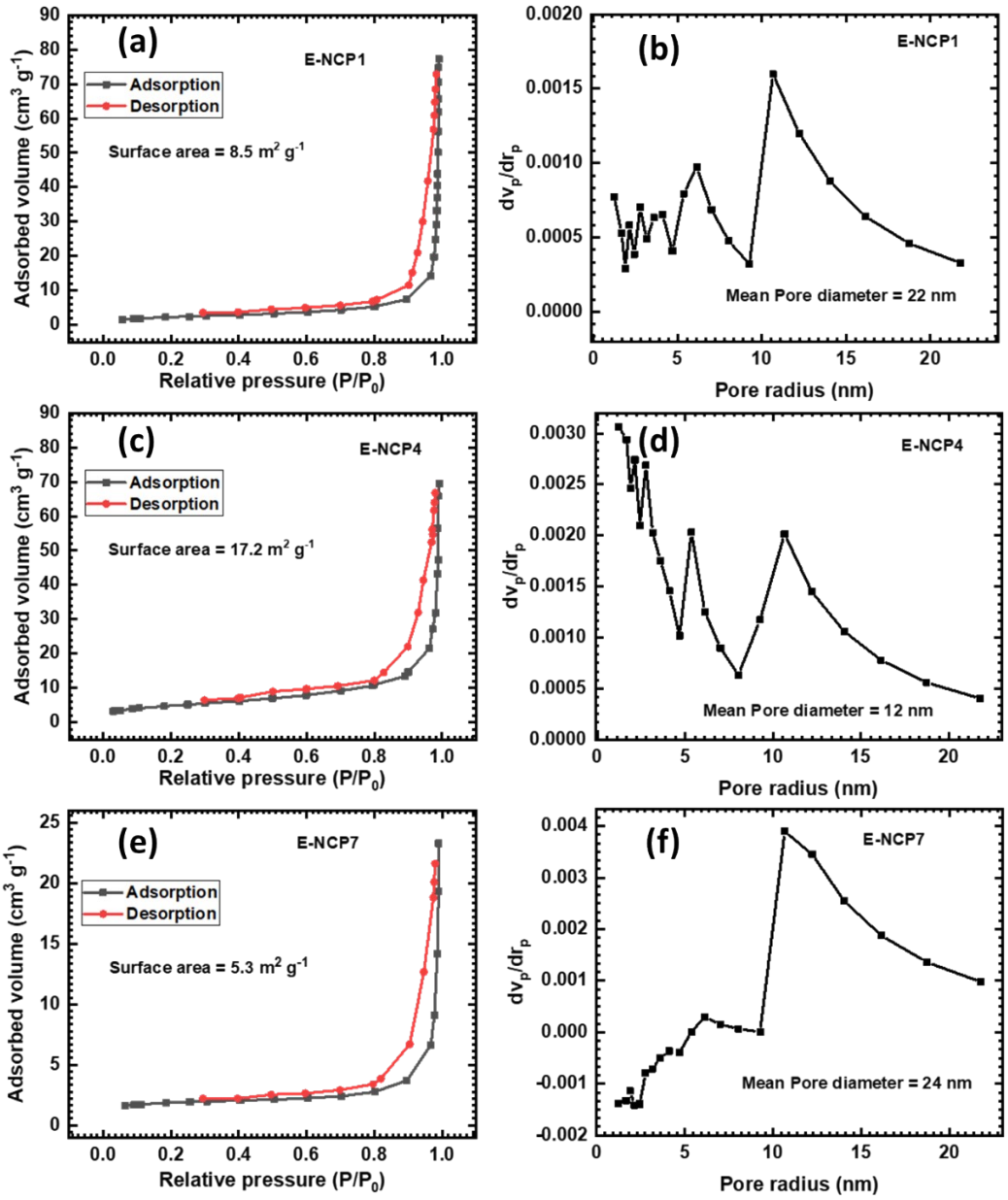

Fig. S6 Nitrogen adsorption/desorption isotherm and pore size distribution of (a, b) E-NCP1, (c, d) E-NCP4 and (e, f) E-NCP7 sample.

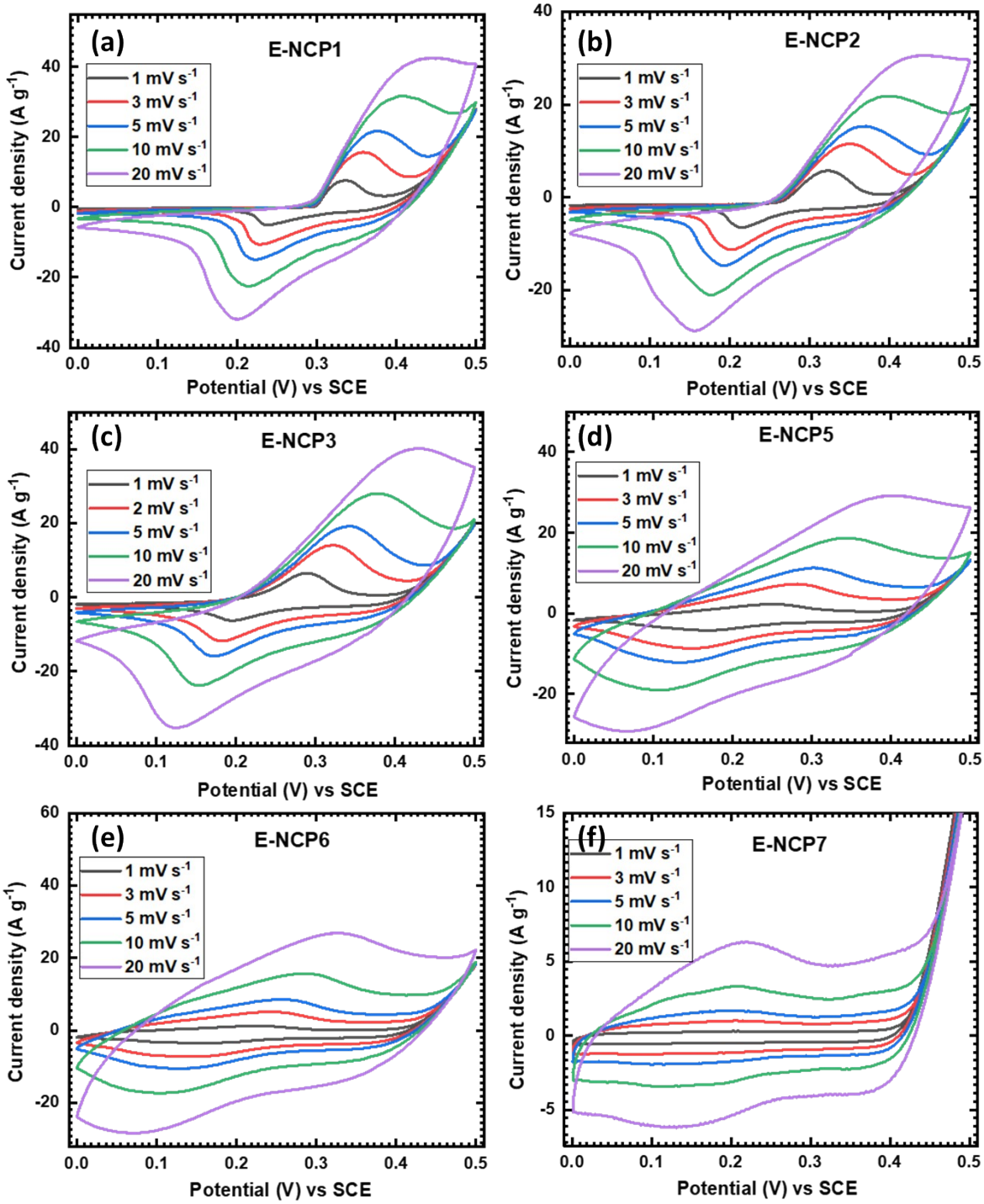

Fig. S7 The CV curves at various scan rates from 1-20 mV s^{-1} for (a) E-NCP1, (b) E-NCP2, (c) E-NCP3, (d) E-NCP5, (e) E-NCP6 and (f) E-NCP7 electrode.

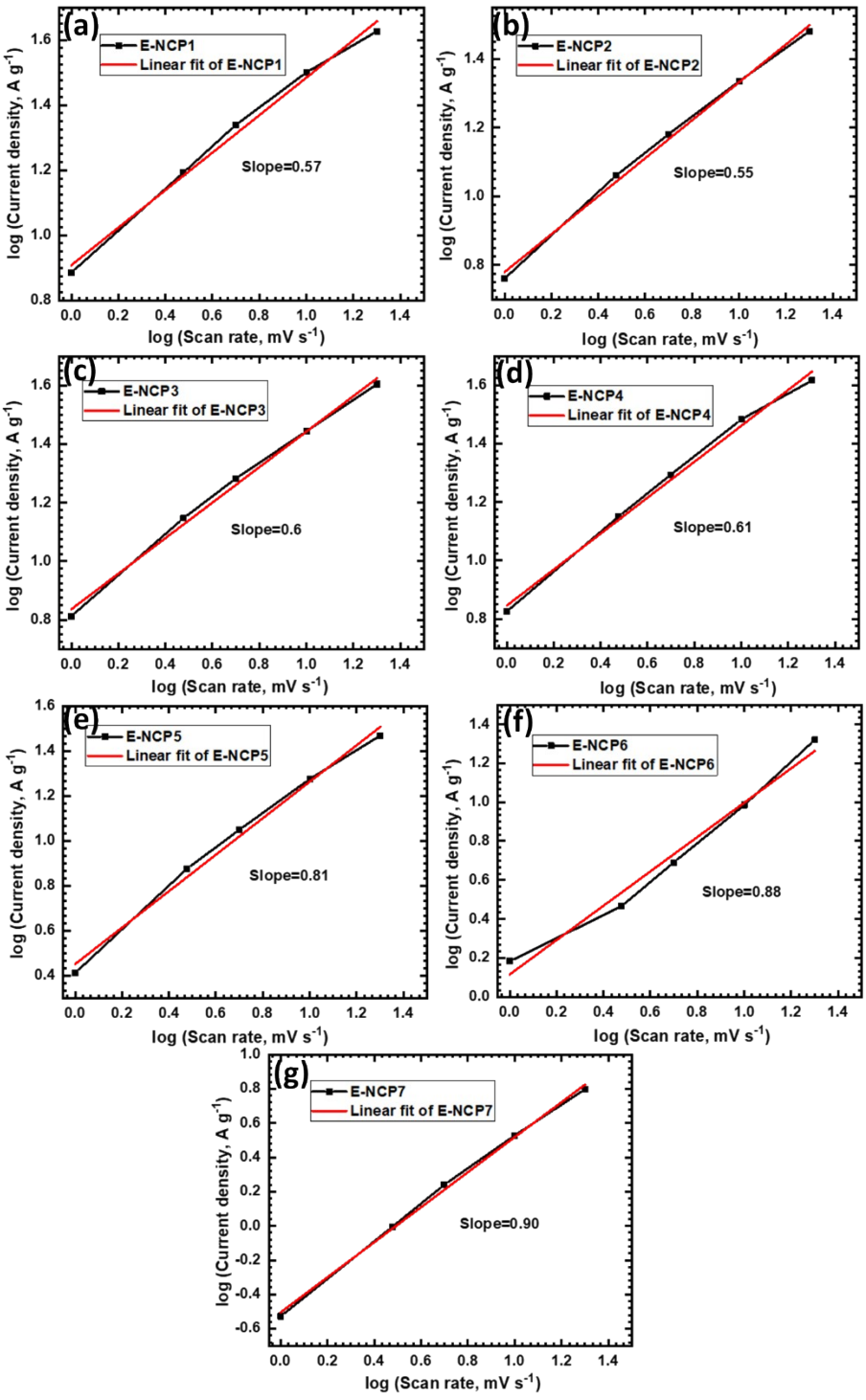

Fig. S8 Plot of log (current density, A g^{-1}) versus log (scan rate, mV s^{-1}) for (a) E-NCP1, (b) E-NCP2, (c) E-NCP3, (d) E-NCP4, (e) E-NCP5, (f) E-NCP6 and (g) E-NCP7 electrode.

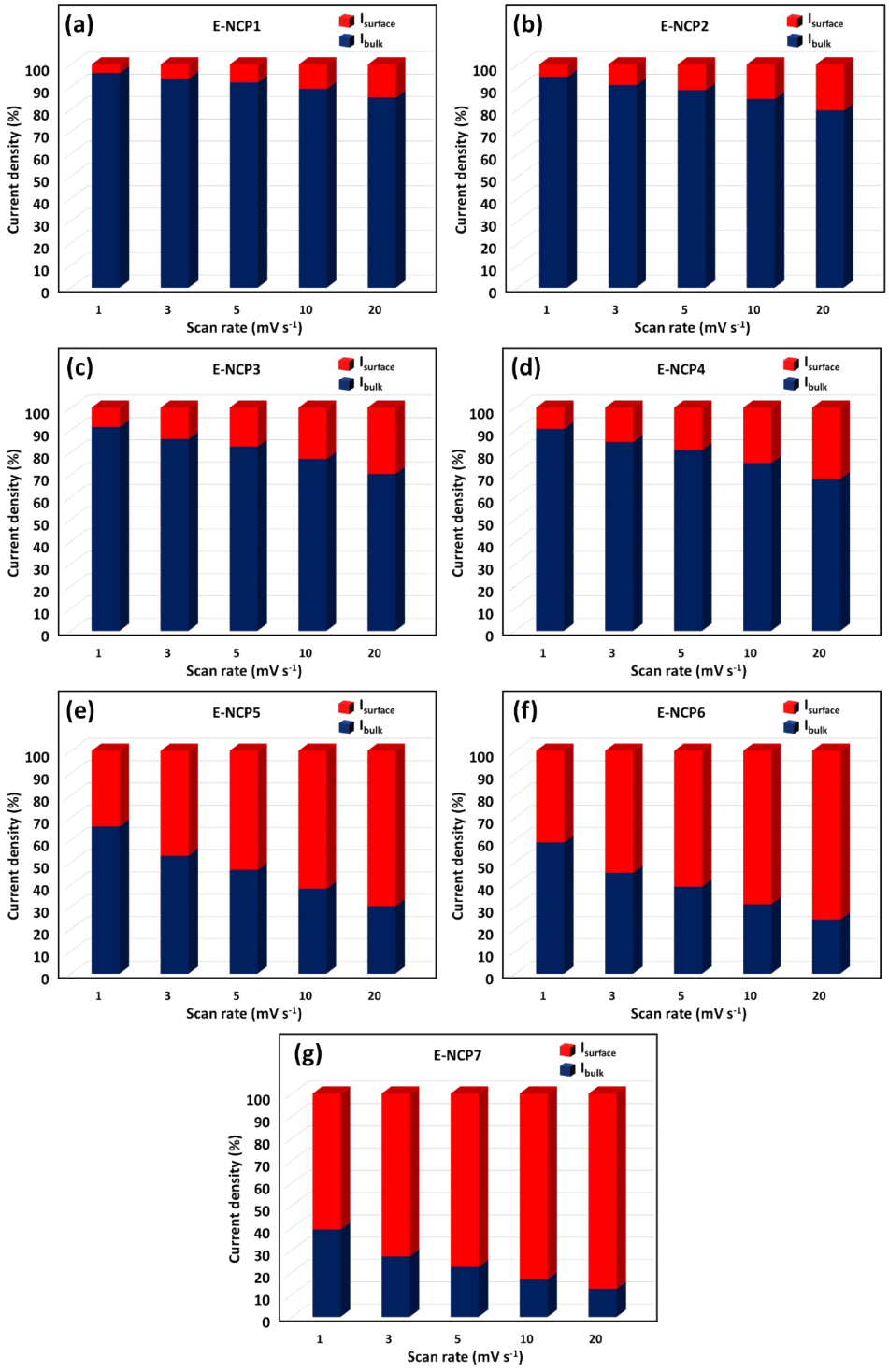

Fig. S9 Graph of calculated contribution of pseudocapacitive (surface current) and battery type (bulk current) current density at various scan rates (1 to 20 mV s^{-1}) for (a) E-NCP1, (b) E-NCP2, (c) E-NCP3, (d) E-NCP4, (e) E-NCP5, (f) E-NCP6 and (g) E-NCP7 electrode.

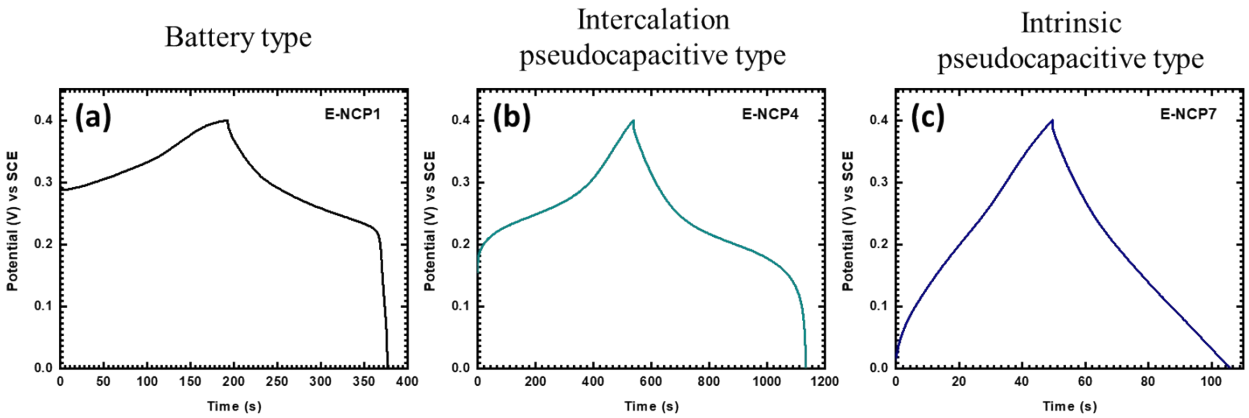

Fig. S10 The GCD curves of (a) E-NCP1, (b) E-NCP4 and (c) E-NCP7 electrode at 1.5 A g^{-1} current density.

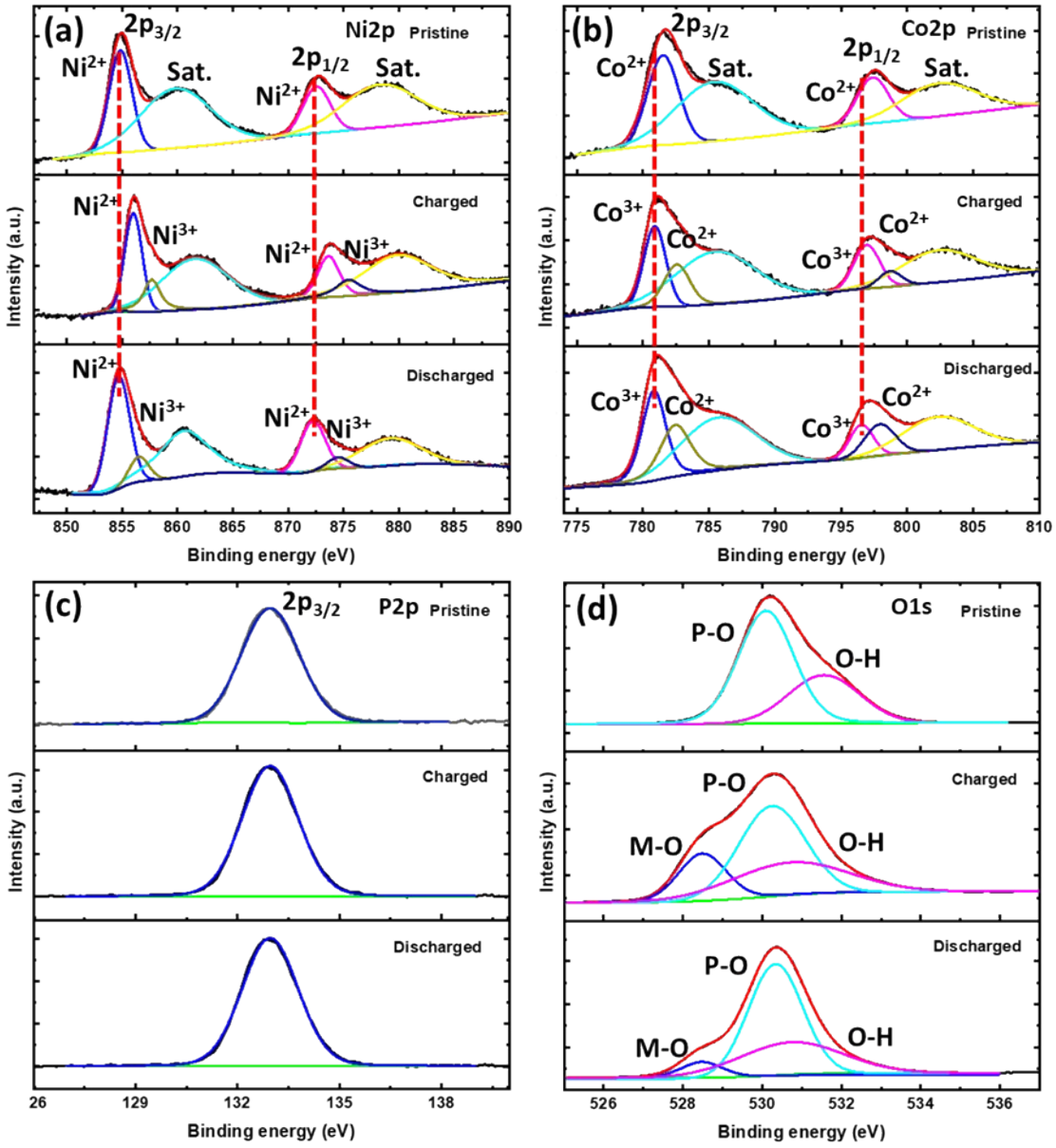

Fig. S11 Comparative XPS (a) Ni2p, (b) Co2p, (c) P2p, and (d) O1s spectra of pristine, charged (0.4 V/SCE) and discharged (0V/SCE) E-NCP4 electrodes.

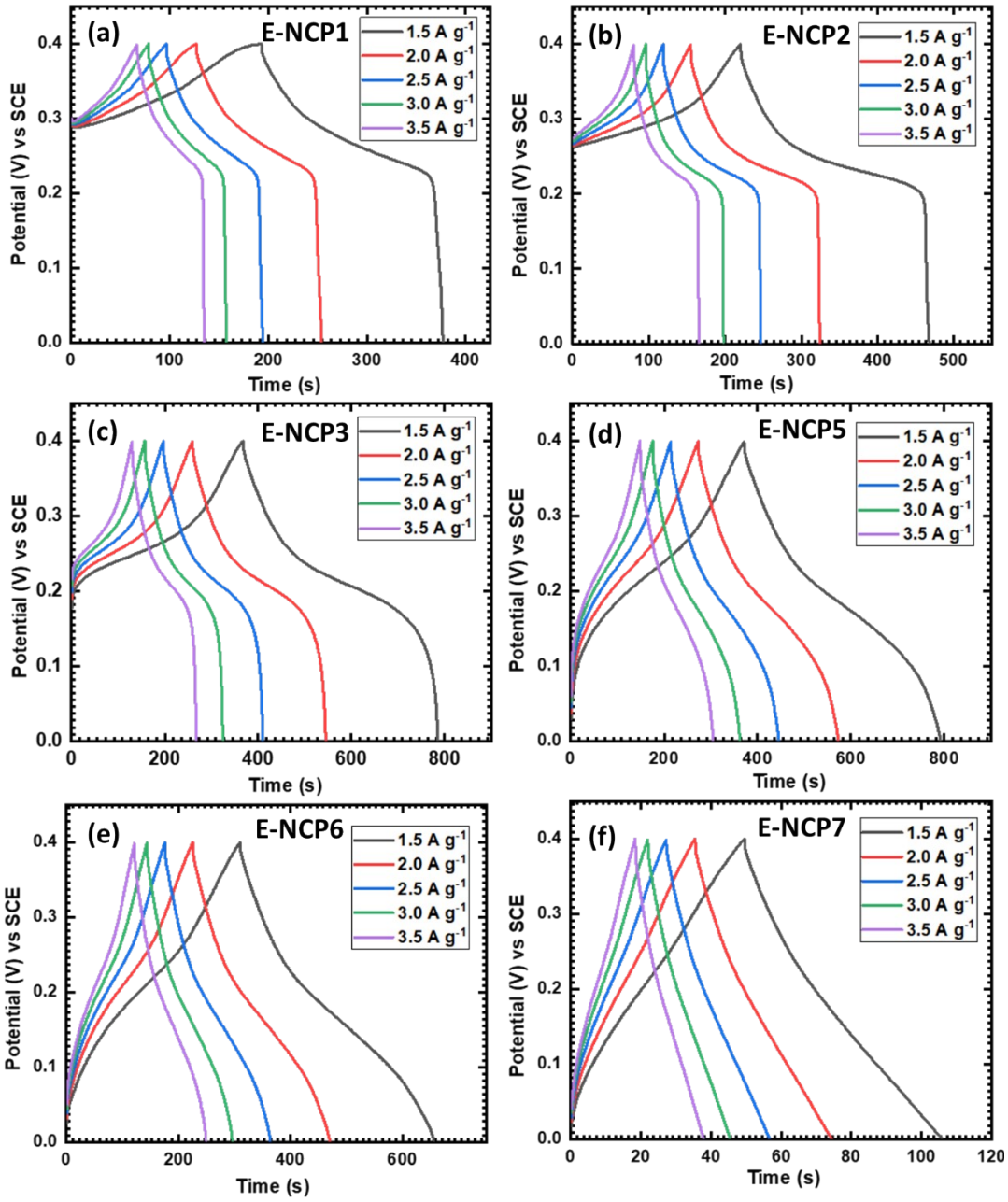

Fig. S12 The GCD curves at various current densities from 1.5-3.5 A g^{-1} for (a) E-NCP1, (b) E-NCP2, (c) E-NCP3, (d) E-NCP5, (e) E-NCP6 and (f) E-NCP7 electrode.

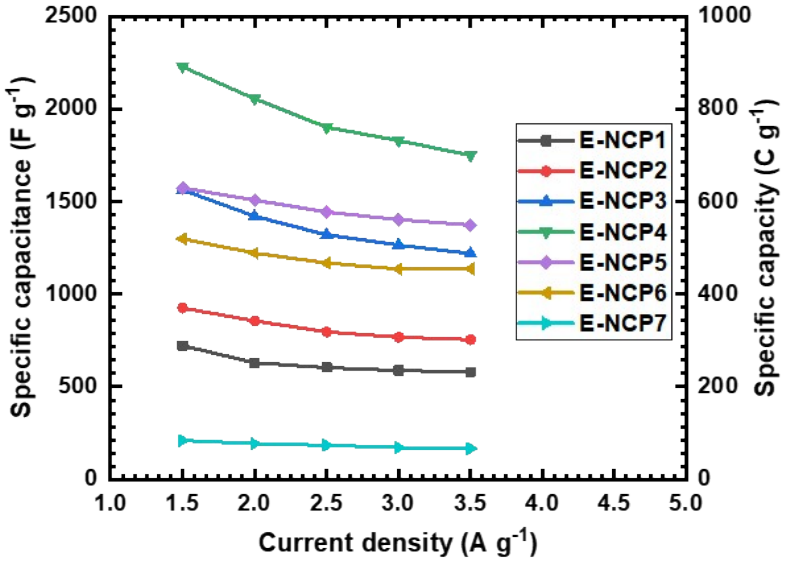

Fig. S13 The plots of specific capacitance and capacity at various current densities for nickel-cobalt phosphate electrodes (E-NCP1 to E-NCP7).

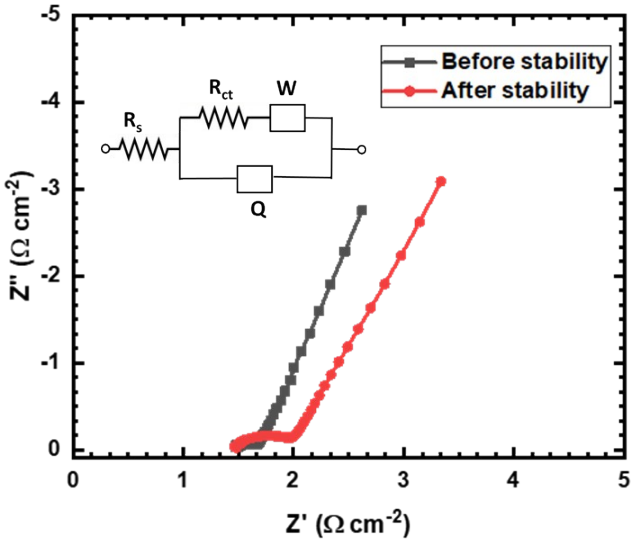

Fig. S14 The Nyquist plots of E-NCP4 electrode before and after 5000 GCD cycles (inset: equivalent circuit).

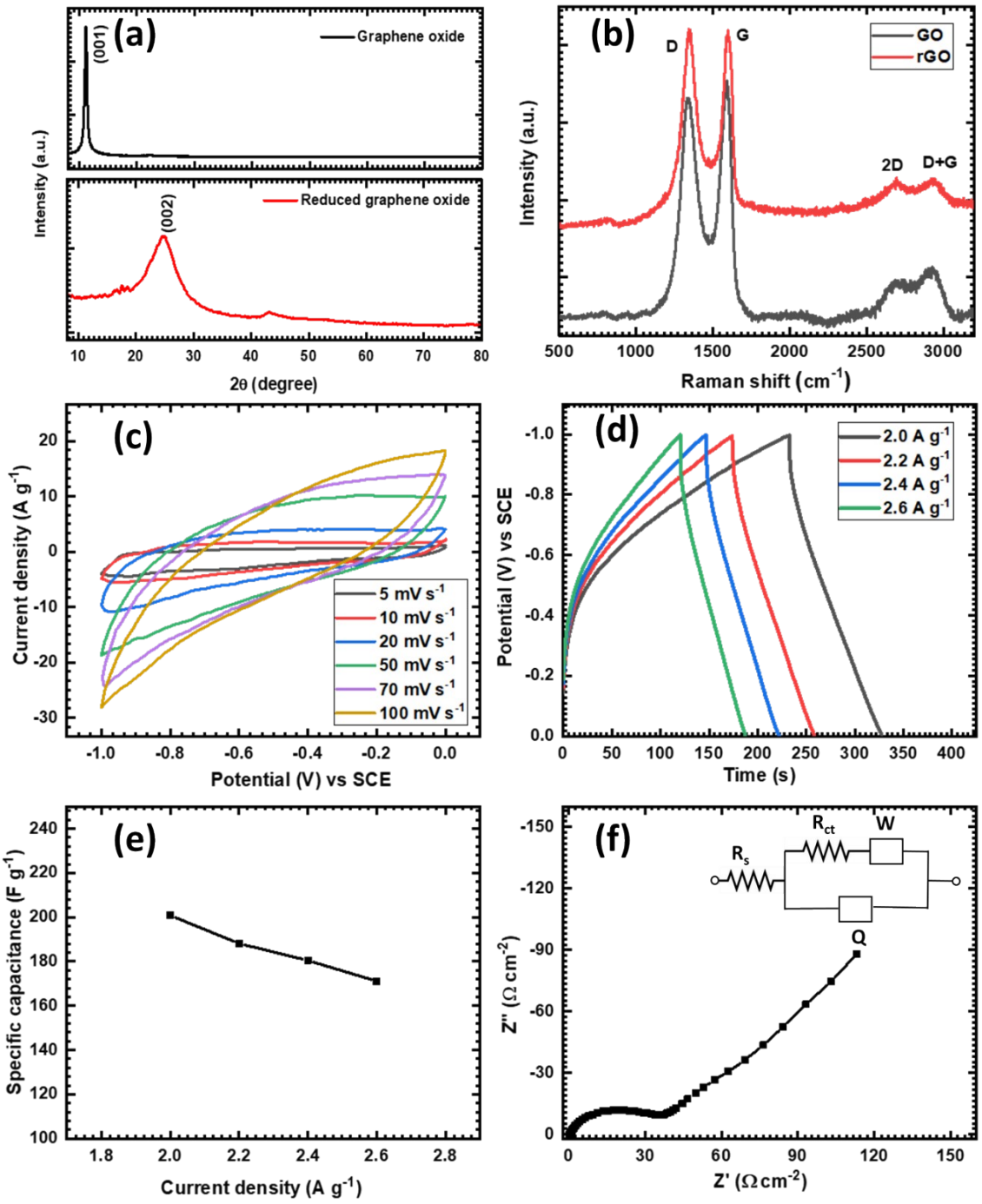

Fig. S15 (a) XRD patterns of GO and rGO samples, (b) Raman spectra of GO and rGO samples, (c) The CV curves at various scan rates from 5-100 mV s^{-1} (d) GCD curves at various current densities from 2.0-2.6 A g^{-1}, (e) specific capacitance at various current densities and (f) Nyquist plot of rGO electrode in 1 M KOH electrolyte.

The XRD patterns and Raman spectra of GO and rGO samples are shown in Fig. S15 (a) and (b), respectively. The XRD and Raman results confirm the successful conversion of GO to rGO by hydrothermal reduction.

The quasi-rectangular shape of CV curves (Fig. S15 (c)) and nearly linear charge-discharge curves (Fig. S15 (d)) confirms EDLC based capacitive nature of rGO electrode. The specific capacitance of 200 F g^{-1} is obtained for rGO electrode at 2 A g^{-1} current density (Fig. S15 (e)). The Nyquist plot of rGO electrode is presented in Fig. S15 (f) with a fitted circuit. The smaller values of R_s and R_{ct} are responsible for higher electrochemical performance of rGO electrode.

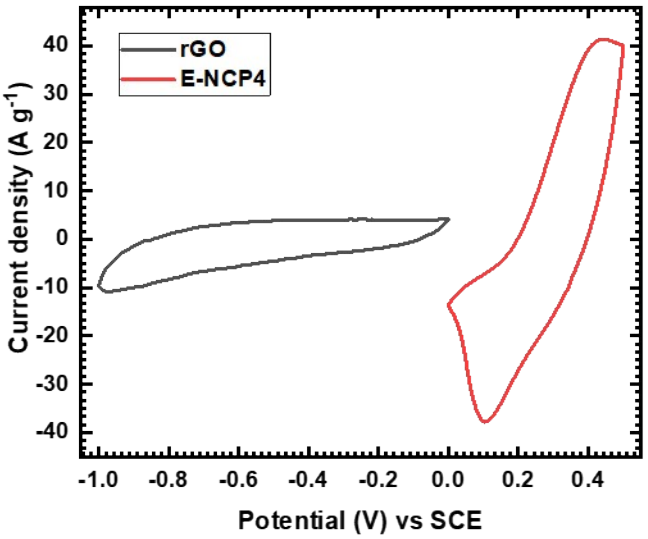

Fig. S16 The CV curves of nickel-cobalt phosphate (E-NCP4) and rGO electrodes at 20 mV s^{-1} scan rate in 1 M KOH electrolyte.

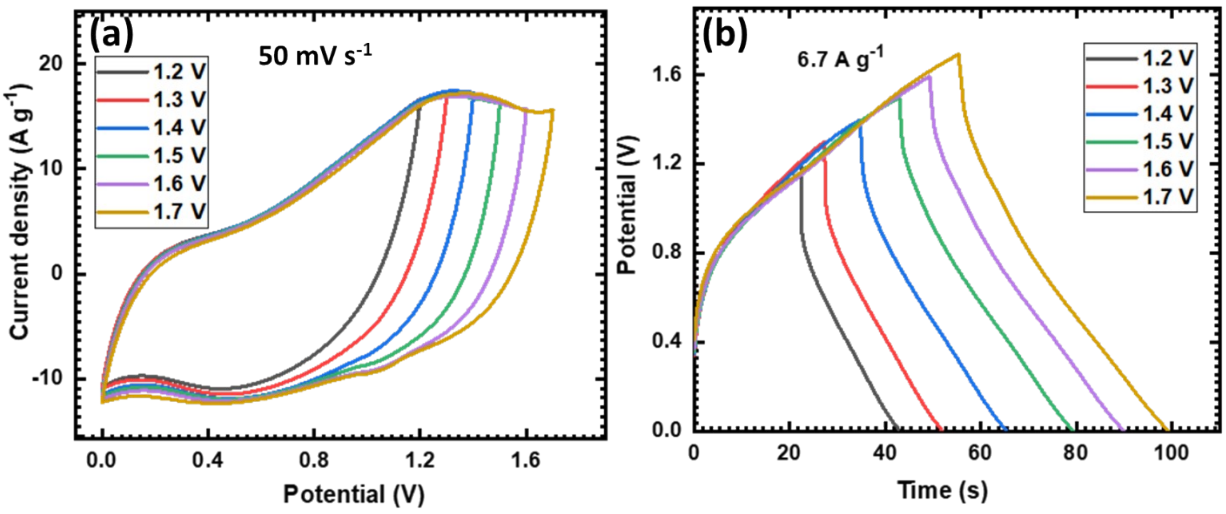

Fig. S17 (a) The CV curves and (b) GCD curves of E-NCP4//rGO AHAS device in different potential windows.

Table S1 Experimental and observed nickel and cobalt atomic ratio in nickel-cobalt phosphate thin film samples (E-NCP1 to E-NCP7).

Sample name	Experimental ratio (Ni:Co)	Observed ratio (Ni:Co)	Obtained phase
E-NCP1	1:0	1:0	$Ni_3(PO_4)_2.8H_2O$
E-NCP2	0.85:0.15	0.81:0.19	$Ni_{2.43}Co_{0.57}(PO_4)_2.8H_2O$
E-NCP3	0.75:0.25	0.76:0.24	$Ni_{2.28}Co_{0.72}(PO_4)_2.8H_2O$
E-NCP4	0.50:0.50	0.48:0.52	$Ni_{1.44}Co_{1.56}(PO_4)_2.8H_2O$
E-NCP5	0.25:0.75	0.30:0.70	$Ni_{0.9}Co_{2.1}(PO_4)_2.8H_2O$
E-NCP6	0.15:0.85	0.09:0.91	$Ni_{0.27}Co_{2.73}(PO_4)_2.8H_2O$
E-NCP7	0:1	0:1	$Co_3(PO_4)_2.8H_2O$

Table S2 Comparison of supercapacitive performance of nickel-cobalt phosphate material with reported literature data.

Sr. No.	Material and morphology	Substrate	Method of deposition	Electrolyte	Capacitance (F g^{-1}) at current density (A g^{-1})	Stability at cycles	Ref.
1.	$Ni_3P_2O_8$-$Co_3P_2O_8.8H_2O$ (Nanoparticles)	Nickel Foam	Co-precipitation	6 M KOH	1980 at 0.5	90.9%, 1000	30
2.	$CoNi_2(PO_4)_2$ (Flowers)	Nickel Foam	Precipitation	2 M KOH	630 C g^{-1} at 1	84.3%, 1000	31
3.	$Co_{0.4}Ni_{1.6}P_2O_7$ (Microplates)	Nickel Foam	Hydrothermal	3 M KOH	1259 at 1.5	88.9%, 1000	32
4.	$NiCoPO_4$ (Nanosheets)	Nickel Foam	Co-precipitation	3 M KOH	1132.5 at 1	93%, 8000	33
5.	$Co_{0.86}Ni_{2.14}(PO_4)_2$ (Nanospheres)	Nickel Foam	Hydrothermal	2 M KOH	1409 at 0.25	-	34
6.	$NiCo_2(PO_4)_2$ (Hollow shells)	Nickel Foam	Microwave assisted	3 M KOH	940.43 at 1	84.5%, 1000	35
7.	$NiCo(PO_4)_3$/Graphene Foam (Flowers)	Nickel Foam	Hydrothermal	1 M KOH	86.4 mAh g^{-1} at 1	-	36
8.	$Ni(Co)NH_4PO_4$@rGO (Microplates)	Nickel Foam	Hydrothermal	6 M KOH	1451 at 1	125%, 5000	37
9.	ZIF-67-LDH-$NiCoPO_4$ (Nanocages)	Nickel Foam	Solvothermal	6 M KOH	1616 at 1	72.46%, 2000	38
10.	$(NH_4)(Ni,Co)PO_4 \cdot 0.67H_2O$ (Microplates)	Nickel Foam	Hydrothermal	6 M KOH	1128 at 0.5	-	39
11.	$NaNi_{0.33}Co_{0.67}PO_4.H_2O$ (Particles)	Nickel Foam	Microwave	1 M KOH	828 at 1	83.1%, 3000	40
12.	$KCo_{0.33}Ni_{0.67}PO_4.H_2O$ (Microplates)	Nickel Foam	Hydrothermal	1 M KOH	1166 at 1.5	94%, 1000	41
13.	Cu/p-CuO/NiCo-P (Nanosheets)	Copper mesh	Electrodeposition	2 M KOH	1768.5 C g^{-1} at 2	92%, 10000	42
14.	$Ni_{1.38}Co_{1.62}(PO_4)_2$ (Microflowers)	Stainless Steel	Chemical bath deposition	1 M KOH	1116 (446 C g^{-1}) at 0.5	75.5%, 3000	43
15.	$NiCoP_4O_{12}$/$(Ni_{0.65}Co_{0.35})_3(PO_4)_2$ (Nanosheets)	Nickel Foam	Electrodeposition	2 M KOH	883 C g^{-1} at 1	-	44
16.	$NiCoO_2$ (Nanoparticles)	Nickel Foam	Solvothermal	3 M KOH	923.2 at 2	-	73
17.	$CoNi_2S_4$	Carbon	Electrodepo	6 M	995.8 C g^{-1} at 2	77.2%,	74

	(Nanospheres/Nanotubes)	fiber cloth	sition	KOH		2000	
18.	Ni-Co-S (Nanosheets)	Ni nanowires	Electrodeposition	6 M KOH	1964 C g^{-1} at 2.5	71%, 2500	75
19.	Ni-Co-S (Nanoparticles)	Ni nanowires	Hydrothermal	6 M KOH	2116 C g^{-1} at 0.725	71%, 2500	76
20.	**$Ni_{1.44}Co_{1.56}(PO_4)_2$ (Microspheres)**	**Stainless Steel**	**Electrodeposition**	**1 M KOH**	**2228 (891 C g^{-1}) at 1.5**	**85%, 5000**	**This work**

Table S3 Electrochemical impedance spectroscopic fitted circuit parameters for Nyquist plots of E-NCP series electrodes.

Sample Name	R_s (Ω cm^{-2})	R_{ct} (Ω cm^{-2})	Q (mF)	n	W (Ω cm^{-2})
E-NCP1	1.31	4.39	2.95	0.631	0.360
E-NCP2	1.44	11.19	0.422	0.695	0.233
E-NCP3	1.87	0.95	0.036	0.702	0.432
E-NCP4	1.47	0.2	9.449	0.771	0.222
E-NCP5	1.75	7.3	191.9	0.806	0.825
E-NCP6	1.33	8.6	229.5	0.842	0.009
E-NCP7	1.25	3.7	118.1	0.856	0.002

Table S4 Electrochemical impedance spectroscopic fitted circuit parameters for Nyquist plots of E-NCP4 electrode before and after 5000 GCD cyclic stability.

Sample	**R_s (Ω cm^{-2})**	**R_{ct} (Ω cm^{-2})**	**Q (mF)**	**n**	**W (Ω cm^{-2})**
Before stability	1.47	0.2	9.44	0.771	0.222
After stability	1.48	0.48	23.3	0.671	0.364

Table S5 Comparative literature study of nickel-cobalt phosphate material as a cathode based asymmetric devices.

Sr. No.	Positive electrode (cathode)	Negative electrode (anode)	Electrolyte	Capacitance (F g^{-1}) at current density (A g^{-1})	Energy density (Wh kg^{-1})	Power density (W kg^{-1})	Stability at cycles	Ref.
1.	$Ni_3P_2O_8$-$Co_3P_2O_8$. $8H_2O$/NF	AC/NF	6 M KOH	94 at 0.5	33.4	399	83%, 5000	30
2.	$CoNi_2(PO_4)_2$/NF	Graphene /NF	2 M KOH	103 at 1	32.2	377.6	-	31
3.	$Co_{0.4}Ni_{1.6}P_2O_7$/NF	AC/NF	3 M KOH	119 at 1	42.2	800	80%, 2000	32
4.	$NiCoPO_4$/NF	AC/NF	3 M KOH	162.8 at 1	32.5	600	80.4%, 5000	33
			PVA-KOH	129.6 at 1	35.8	700	90.5%, 5000	
5.	$Co_{0.86}Ni_{2.14}(PO_4)_2$/NF	AC/NF	-	149.6 at 0.7 mA	45.8	42.4	57.8%, 2500	34
6.	$NiCo(PO_4)_3$/Graphene Foam/NF	AC/NF	1 M KOH	45 mAh g^{-1} at 0.5	34.8	377	95.5%, 10000	37
7.	ZIF-67-LDH-$NiCoPO_4$/NF	AC/NF	PVA-KOH	116.67 at 0.1	33.29	150	67.24%, 10000	38
8.	(NH_4) $(Ni,Co)PO_4 \cdot 0.67H_2O$ /NF	HPC/NF	6 M KOH	88 at 0.01	35.3	101	95.6%, 5000	39
9.	$NaNi_{0.33}Co_{0.67}PO_4$. H_2O/NF	Graphene /NF	1 M KOH	95.52 at 0.5	29.85	374.95	76.9%, 10000	40
10.	$KCo_{0.33}Ni_{0.67}$ $PO_4.H_2O$/NF	AC/NF	1 M KOH	227 at 1.5	80.64	1200	82%, 5000	41
11.	Cu/p-CuO/NiCo-P	3DPG	2 M KOH	247.78 at 1	88.1	800.6	89%, 10000	42
12.	$Ni_{1.38}Co_{1.62}(PO_4)_2$/SS	rGO/SS	1 M KOH	120 at 1.3	43.3	1000	80%, 4000	43
			PVA-KOH	102 at 0.2	36.2	160	83.7%, 4000	
13.	$NiCoP_4O_{12}$/ $(Ni_{0.65}Co_{0.35})_3(PO_4)_2$/ NF	AC/NF	2 M KOH	119.4 at 3	54	2700	81%, 10000	44
14.	$CoNi_2S_4$/CNF	rGO-CNTs	6 M KOH	112 at 4	35	3000	96.9%, 10000	74
15.	Ni@Ni-Co-S/Graphite paper	rGO-CNTs/ Graphite	6 M KOH	53.9 at 0.31	16.8	232.9	90.5%, 10000	75

		paper						
16.	Ni@Ni-Co-S/Graphite paper	rGO-CNTs/Graphite paper	6 M KOH	143 F cm^{-3} at 0.5 A cm^{-3}	44.5 mWh cm^{-3}	375 mW cm^{-3}	96.9%, 5000	76
17.	**$Ni_{1.44}Co_{1.56}(PO_4)_2$/SS**	**rGO/SS**	**1 M KOH**	**185 at 2.7**	**65.2**	**2200**	**97%, 4000**	**This work**
			PVA-KOH	**90 at 0.4**	**32**	**320**	**88%, 4000**	

References

S1 D. Marcano, D. Kosynkin, J. Berlin, A. Sinitskii, Z. Sun, A. Slesarev, L. Alemany, W. Lu, J. Tour, *ACS Nano*, 2010, **4**, 4806-4814.

S2 P. Katkar, S. Marje, S. Pujari, S. Khalate, A. Lokhande, U. Patil, *ACS Sustain. Chem. Eng*., 2019, **7**, 11205-11218.